EGTRIB Journal
JOURNAL OF
THE EGYPTIAN SOCIETY OF TRIBOLOGY
VOLUME 20, No. 3, July 2023, pp. 95 - 108 **ISSN 2090 - 5882**
(Received June 01. 2023, Accepted in final form June 23. 2023) **jest.journals.ekb.eg**

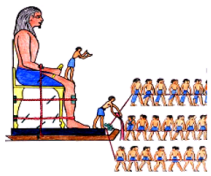

EFFECT OF MULTI-PASS SHIELDED METAL ARC WELDING ON MICROSTRUCTURE CHARACTERIZATION AND MECHANICAL PROPERTIES OF 2507 SUPER DUPLEX STAINLESS STEEL

Ali A. S.[1], Mohamed M. El-Sayed Seleman[2], Mohamed M. Z. Ahmed[2,3], Elsoeudy R. I.[1], Eslam Abd Elaal Mahmoud[4] and Elzayady N.[5]

[1]Mechanical Engineering Dept., Faculty of Engineering, Suez Canal University, EGYPT.
[2] Department of Metallurgical and Materials Engineering, Faculty of Petroleum and Mining Engineering, Suez University, Suez 43512, Egypt.
[3] Mechanical Engineering Dep., College of Engineering at Al Kharj, Prince Sattam Bin Abdulaziz University, Al Kharj 16273, Saudi Arabia.
[4] Siemens-energy Company, Cairo, Egypt
[5] Mechanical and Aerospace Department, Institute of Aviation Engineering and Technology,Giza, EGYPT.

ABSTRACT
The present work investigates the weldability, microstructure, and mechanical properties of 6 mm thick 2507 super duplex stainless steel were welded by multi-pass shielded metal arc welding technique (SMAW) with ER2595 electrode using different heat inputs. The produced joint was characterized and evaluated by using radiographic inspection, liquid penetrant test, scanning electron microscopy, optical microscopy, hardness and tensile test. The results obtained demonstrated that the filler electrode, heat inputs and interpass temperature are the parameters control for produce of defect-free joint. The 2507 SDSS shielded metal arc welding show an improvement in hardness and yield strength compared to the base metal. The weld zone exhibited four distinct morphologies of austenite including secondary austenite (SA), Widmanstatten austenite (WA), intra-granular austenite (IGA), and grain boundary austenite (GBA), in addition to the presence of ferrite. The ferrite content in the weld zone remained close to the balance ratio of base metal and showed no significant variation when using different welding parameters.

KEYWORDS
2507 SDSS, mechanical properties, microstructure; SMAW, ferrite content.

INTRODUCTION
Super duplex stainless steels (SDSS) of SAF2507 have gained significant attention in various industries such as Mining, marine, power stations, petrochemical, and other industries, [1–5]. 2507- SDSS characterized by its balanced composition of ferrite (α) and austenite (γ), [6–8], offers several distinct advantages in various applications.

Furthermore, the equal distribution of these two phases contributes to a unique combination of the material's mechanical properties. The ferrite phase contributes to the steel's high strength and toughness, making it capable of withstanding high loads and impacts. The austenite phase provides improved ductility and formability, allowing for ease of fabrication and shaping, [9, 10]. The combination of these mechanical properties makes super duplex stainless steel suitable for structural components, pressure vessels, and piping systems in demanding industries.

SAF 2507 super duplex stainless steel also demonstrates good thermal conductivity and low thermal expansion, providing enhanced heat transfer capabilities and dimensional stability in high-temperature applications, [11]. This attribute is valuable in vessels, heat exchangers, boilers, and other thermal processing equipment, [12]. welding these alloys presents unique challenges due to their complex microstructure and susceptibility to thermal distortion and solidification cracking, [13]. However, the selection of an appropriate welding technique is critical to maintain the desired properties of the welded joints, [14].

Fusion welding processes such as gas metal arc welding (GMAW), shielded metal arc welding (SMAW), flux cored arc welding (FCAW), and gas tungsten arc welding (GTAW) can all be used to weld the 2507-SDSS alloy 2507 SDSS, [15 - 18]. Among these processes, the SMAW technique is distinguished by its ability to produce efficient welds. In addition, the SMAW weldments of 2507-SDSS indicate an acceptable ratio of γ/α by selecting the suitable welding parameters, joint design, and filler rod materials, [18]. SMAW offers several advantages for welding duplex stainless steel due to its versatility, simplicity, and suitability for various applications, [19].

In addition, SMAW is particularly advantageous for welding super duplex stainless steel due to its ability to provide a stable arc even in challenging positions and environments. The process offers excellent control over the heat input, which is crucial for preventing excessive heat and preserving the microstructural integrity of the super duplex stainless steel, [18]. Moreover, SMAW allows for efficient deposition of filler metal, resulting in strong and reliable weld, [20 - 26].

However, SMAW welding of stainless steel requires careful consideration of parameters such as electrode selection, current and voltage settings, travel speed, and preheat/post-weld heat treatment, [27 - 29]. Proper electrode selection, typically choosing a duplex stainless steel electrode, ensures a compatible composition and mechanical properties between the filler metal and the base metal. Appropriate adjustment of current, voltage, and travel speed achieves a balanced heat input, [8]. In this respect, Gupta et al., [18] studied the effect of heat input on mechanical properties and microstructure characterization which welded by SMAW of 2507 SDSS 5.5 mm thick plate. The E2595 electrode was used in the SMAW process to weld two samples with varying heat inputs: 0.54 kJ/mm, 1.10kJ/mm. The microstructure examinations, including optical microscope and scanning electron microscopy, revealed minimal differences in the heat affected zone (HAZ) between the two heat

inputs. Furthermore, both weldments demonstrated comparable mechanical properties.

The present work aims to evaluate the effect of multi pass SMAW parameter on the welding of 6 mm thick plate 2507-SDSS and their impact on the microstructure and mechanical properties of the weldment.

EXPERIMENTAL

Material

A 6 mm thickness SAF 2507-SDSS plates were utilized as initial materials with 200 mm length, and 100 mm width. The 2507-SDSS plates were supplied by RAHUL Company, Bogra, Bangladesh. The chemical composition of SAF2507-SDSS is presents in Table 1 according to the supplier.

Table 1. chemical composition of SAF2507-SDSS.

Element	Ni	Cr	Mo	Mn	Si	P	C	S	Fe
(wt. %)	8	26	5	1.2	0.8	0.035	0.03	0.02	Bal.

SMAW Procedure of SAF2507-SDSS

The SMAW method has been utilized for the entire welding procedure; root, filling, and final passes with the filler rod of ER2595 filler metal with a diameter of 2.5 mm. The SMAW of the 2507-SDSS procedure was done according to ASME code section IX using the manual SMAW machine model Magmaweld RS 500 M, Istanbul, turkia. Because excessive heating has harmful influences on the properties of the welded SDSS alloys, [11], preheating was exempted. And the maximum temperature of the SMAW inter-pass involved was less than 110 °C, as suggested to minimize precipitations of the intermetallic phases. Table 2 shows the composition of the ER2595 welding consumables rod. Compared to the 2507-SDSS, the filler rod of ER2595 has a 0.84 % more nickel than the initial SDSS plates to form γ from solid delta α, [30]. Figure 1 displays a schematic drawing of the 2507-SDSS butt weld joint design; V- groove shape with an angle of 60^0, a root face of 2 mm, and a root gap of 4 mm. with multi- pass of SMAW. Table 3 lists the SMAW of the 2507-SDSS details. A manual stainless steel brush was applied to remove oxides scales during the SMAW process.

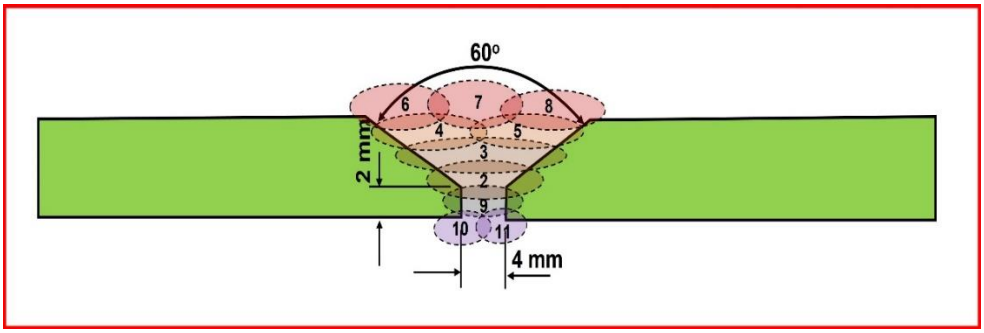

Fig. 1 Joint configuration of the 2507-SDSS for the SMAW process.

Table 2 The nominal composition of the ER2595 (in wt. %).

Element	Ni	Cr	Mo	Mn	Si	C	P	S	Fe
Content (wt. %).	8.84	25.31	3.35	1.07	0.53	0.33	0.013	0.012	Bal.

Table 3 SMAW welding parameter.

Pass No.	Interpass temp. ^{o}C	Electrode	Amps	Volt	Travel speed mm/min	Heat input J/mm
1	-	ER2595 – 2.5 mm diameter	76	28	107	1192
2	70		79	25.4	291	414
3	80		78	26	210	579
4	105		78	26	200	608
5	110		78	26	185	658
6	95		80	25	240	500
7	85		81	24.5	251	476
8	90		81	25	245	496
9	60		81	25.2	200	612
10	90		80	24.5	240	490
11	95		79	24.8	250	515

Evaluation and characterization of welded joints

After SMAW technique, the nondestructive tests of visual inspection, liquid penetrant test, and the radiographic test were utilized to identify any welding defects present on both the surface and internal regions of the welded joint. Visual inspection allows for real-time evaluation of the surface condition, it enables the identification of visible defects, such as large cracks, corrosion, surface irregularities, or improper welds, which can be addressed promptly before they worsen. The liquid penetrant test, also known as dye penetrant test, used to detect surface defects of surface of welded joints such as cracks, surface porosity and discontinuities in materials. The radiographic test used to examine the internal structure of materials for defects or discontinuities. After applied the non-destructive tests, the welded joint was sectioned perpendicular to the welding direction using a wire cut machine, for the microstructure, macrostructure, hardness, and tensile test. The polished cross-section of the joint was subjected to optical microstructure analysis using eicher solution of CuCl2 in a mixture of 100 mL of HCl and 100 mL of ethanol, the specimens were immersed in this solution for a duration of 25 second. The SEM analysis for the welded joint was done using field emission scanning electron microscopy. As for phase analysis in the weld zone, α and γ phases are determined by using a ferrite scope. The Vickers hardness test was performed on the cross-section of the welded joint using a load of 2000 gf, dwell time of 15 seconds. Tensile specimens were extracted in a direction

perpendicular to the welding direction and prepared in accordance with the ASTM E8/E8M-16a standard, [31]. The tensile test specimen dimensions are presented in Fig. 2. The tensile test was conducted at room temperature, utilizing a universal test machine with ram head-speed of 0.5 mm/min.

RESULTS AND DISCUSSION

Nondestructive inspection Results.

Fig. 3a presents the top view of 2507 SDSS with multi pass SMAWed. By visual inspection It is clear that the obtained joint using the design V- groove shape with an angle of 60^0, a root face of 2 mm, and a root gap of 4 mm, no defects are detected indicating excellent surface appearance of multi pass SMAW. Figure 3(b, c) shows the liquid penetration test and radiography images, respectively of the welding joint after SMAW. For liquid penetration test it was observed that, very good appearance of the welded surface, good surface conditions without any surface defect detected. On the other hand, radiography image indicated that no internal defects detected along the joint length that is due to suitable joint design, suitable welding parameters, and adequate material flow.

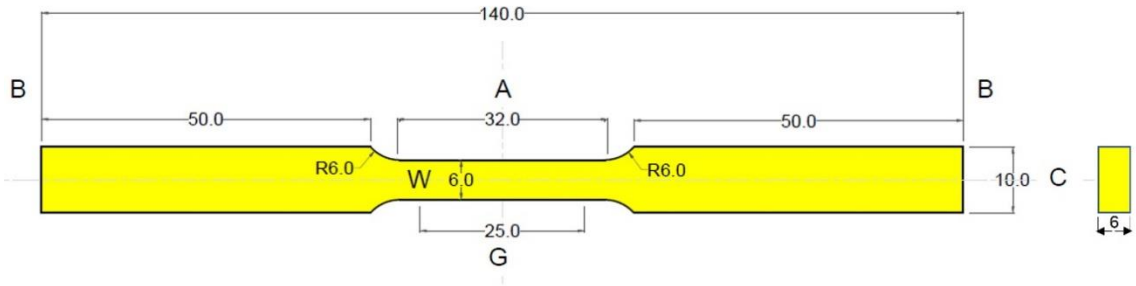

Where:

G: Gage length
W: Width
T: Thickness
R: Radius of fillet
L: Overall length
A: length of reduced section
B: length of grip section
C: Width of grip section

Fig. 2 Tensile test specimen Dimensions according to ASTM E8/E8M-16a; all dimensions in mm.

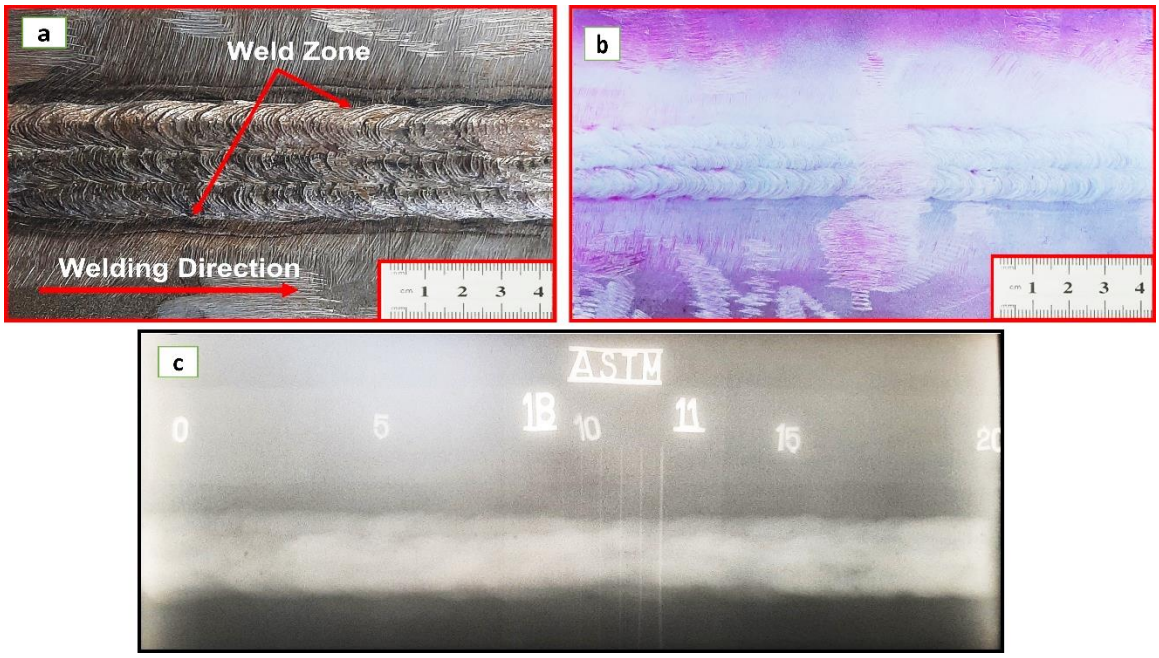

Fig. 3 (a) Top view of 2507 SDSS with multi pass SMAW, (b) image for liquid penetration test of 2507 SDSS with multi pass SMAW, (c) Radiographic images of the 2507 with multi pass SMAW.

Macrostructure and Microstructure characterization

Figure 4a illustrates the macrostructure image of the transverse cross-section of the SMAWed joint. It is clear that by employing a V-shaped groove with a 2 mm root face and a 4 mm root gap, a defect-free joint was obtained by using multi pass SMAW. Figure 4b presents the optical microstructure of the BM for 2507 SDSS where both ferrite (α) and austenite (γ) are easily identified. Moreover, the fusion welding characteristics of the welded joint reveal the presence of two distinct zones, the weld zone (WZ) and the heat-affected zone (HAZ), [18]. Some microstructural changes take place in the WZ region resulting in secondary austenite clusters (SA), inter-granular austenite (IGA), grains boundaries austinite (GBA) and Widmanstätten austenite (WA) as shown in figure 4 c. The different welding zones with different magnifications are shows in figure 4 (d, e). It is important to note that achieving the desired microstructure in the weld zone is crucial for maintaining the mechanical and corrosion-resistant properties of the 2507 SDSS. Careful control of welding parameters, including heat input and cooling rate, is necessary to optimize the microstructural features and ensure the integrity of the welded joint. During the SMAW process, the high temperatures reached during welding cause the austenite to transform into a coarser grain structure. This can lead to the formation of Widmanstätten austenite (WA), which appears as elongated or lath-like structures. The microstructure of HAZ comprises large grains of α-phase with interconnected γ phase networks on α grains boundaries (GBA) and smaller grains of Widmanstatten austenite (WA). Additionally, there is presence of intra-granular and grain boundary austenite (IGA), which form within the ferrite grains. The formation of secondary austenite clusters (SA) were also observed in some of the reheating areas especially in

the third and fourth passes, [18]. Widmanstatten austenite (WA), secondary austenite clusters (SA), intra-granular austenite (IGA) and grain boundaries austenite (GBA) are significant features of the microstructure for all heat inputs [18, 32 - 33]. For the current investigations, no intermetallic are observed in the weld zone across all the applied heat inputs.

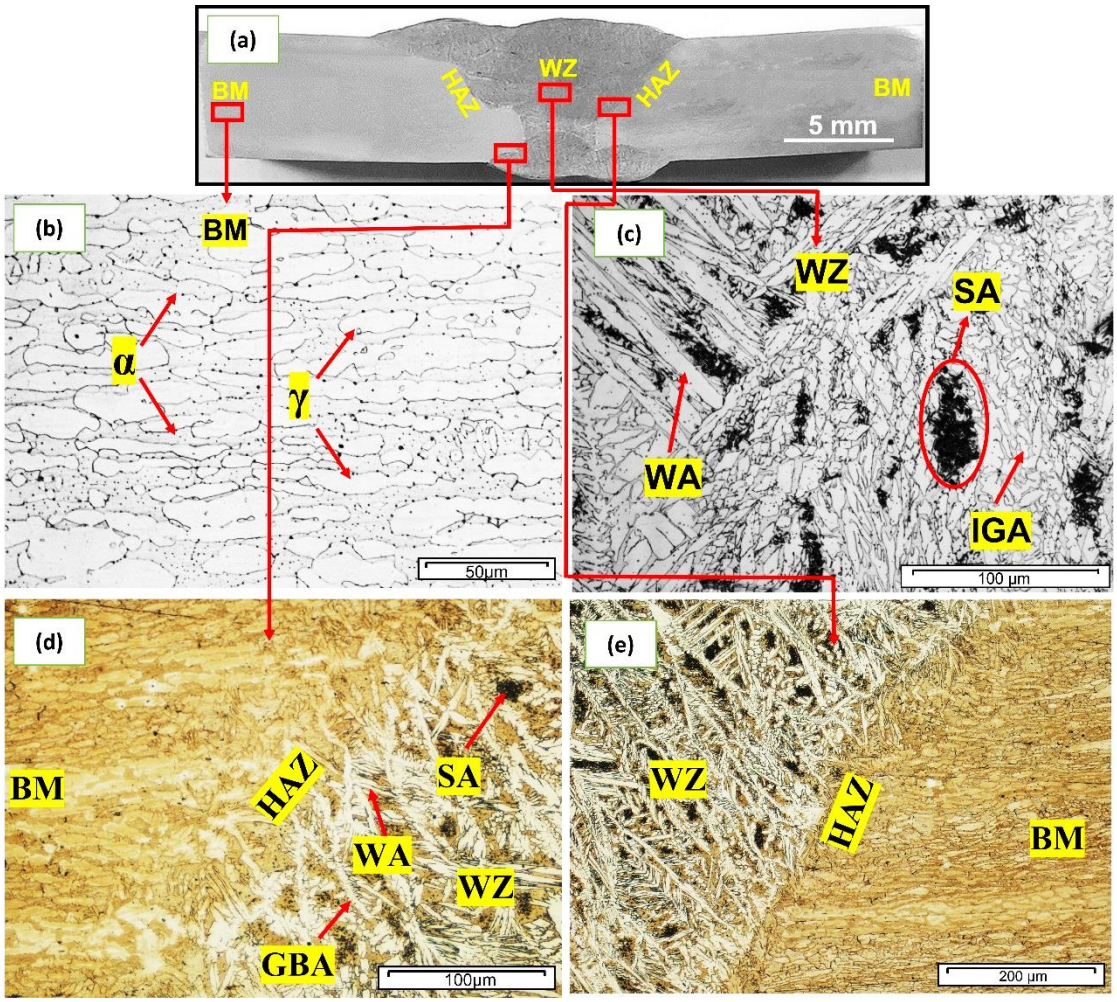

Fig. 4 (a) Macrostructure image of 2507 SDSS with multi pass SMAWed joint, (b) Optical microstructure image of the BM, (c) Optical microstructure image of WZ, (d, e) Optical Microstructural images of the various zones for SMAWed joint.

3.3 Ferrite / austenite content

Figure 5 presents the percentage of α content during measurement by using a ferrite-scope for the weld joint of 2507 SDSS produced through the multi pass SMAW technique. Table 4 shows the ferrite reading content measurement of welded joint of 2507 SDSS with multi pass SMAW. The measurements reveal that in the base metal (BM), the α and γ percentage phases are 50.6% and 49.4%, respectively. These findings align closely with previous reports by other authors on the as-received 2507 SDSS [17,18,34]. Furthermore, α and γ percentage phases for the SMAWed joint are

47% and 53 % respectively. These phase ratios are relatively close to the equilibrium ratio of α and γ in the BM. According to previous reports, The welded joint could be classified as a high-quality joint when the proportion of the γ phase in the DSS welded joint exceeds 30%, [33]. The weld zone of the SMAWed joint exhibits a slightly higher austenite proportion (53%) compared to the BM (47%). This increase can be ascribed to the utilization of ER2595 wire during the welding process, which contains a higher nickel content than the 2507 SDDS. Meanwhile, the multi pass SMAW technique which applied in this study maintained α and γ phases without inducing ferritization. Therefore, these results endorse the use of multi pass SMAW for welding 2507 SDSS, specifically under the recommended welding conditions established in the current work, while preserving the desired α:γ ratio.

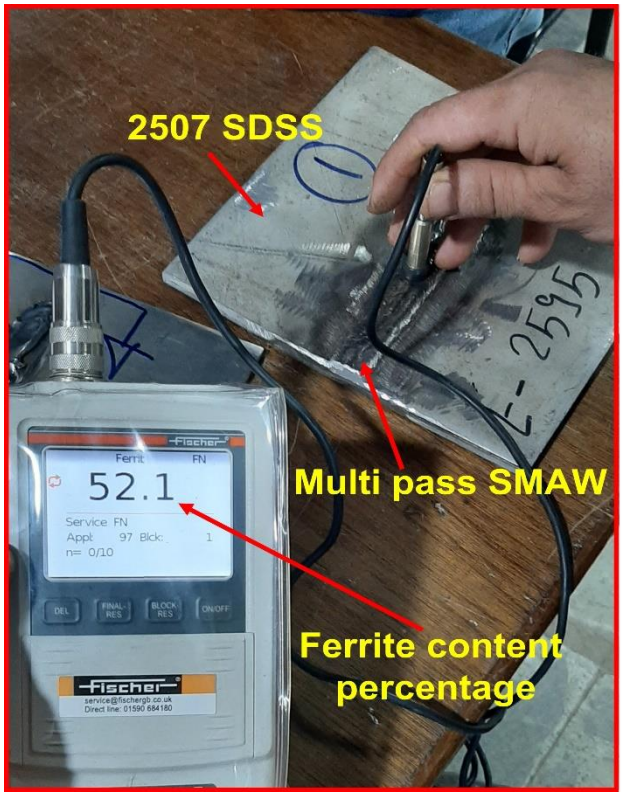

Fig. 5 Ferrite content percentage during measurement by using a ferrite-scope.

Table 4 Ferrite content measurements for 2507 SDSS BM, WZ of the SMAWed joint.

Samples	Readings of ferrite No. (%)					AV. Reading of α phase (%)	Calculated γ Phase (%)
Base Metal	52	51	48	51	51	50.6	49.4
SMAW	52.1	46	45	49	42.9	47	53

Hardness and tensile characteristics

Figure 6 illustrates the hardness profile of the 2507 SDSS produced through the multi pass SMAWed. The hardness measurements were taken along two transverse lines in the cross-section of the welded joints. It is evident that the maximum hardness values reach up to 369 HV at the center of the stir zone. The hardness gradually decreases as we move to the HAZ, with value of 272.1 HV. Compared to the as-received base material (BM), the hardness value is 319 HV. The variations in hardness within the weld zone can be attributed to differences in the microstructure, particularly in terms of the morphology and distribution of micro-constituents, [18]. The presence of a higher proportion of the γ phase contributes to an improvement in the hardness of the WZ, [10, 35] . Conversely, the presence of significantly coarser ferrite grains in HAZ leads to a decrease in hardness.

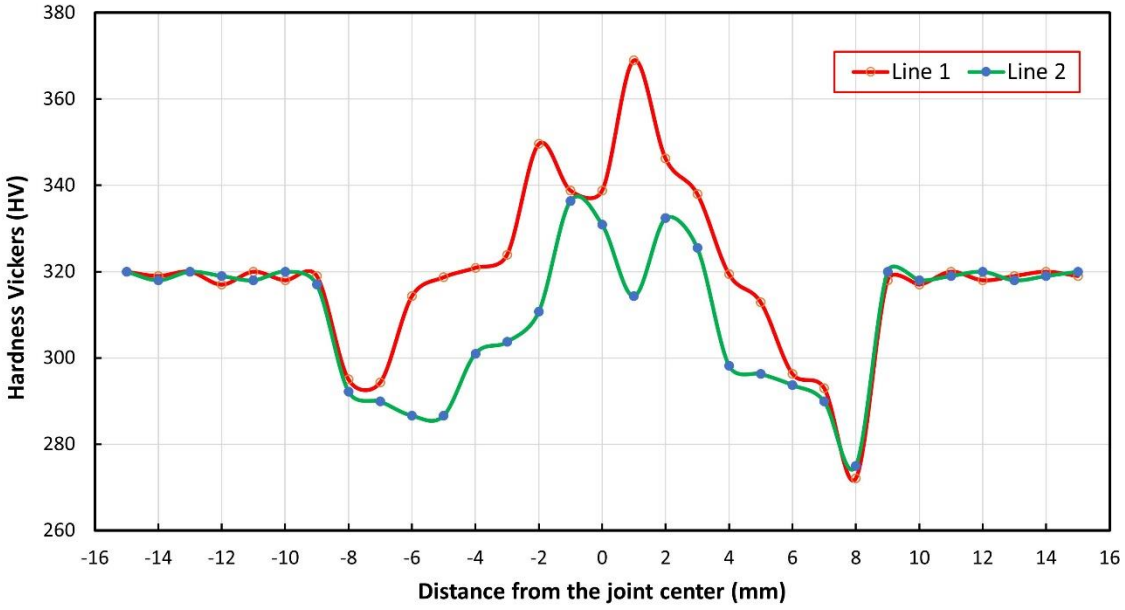

Fig. 6 Vickers hardness measurements of the 2507 SDSS SMAWed joint.

Figure 7 (a, b) shows the tensile test specimen of the BM and SMAWed joint before the test. After conducting the test, figure (c) displays the fracture location occurred at the HAZ indicated in the red circle. Tensile properties including ultimate tensile stress (UTS), yield stress (YS), and elongation (E%) for the SMAWed joint, compared to the BM are shown in Fig. 8. it is clearly obtained that the UTS value for BM sample of 1273 MPa is relatively close to the SMAWed sample value of 1244 MPa. the E% values for BM sample is 50 % which is larger than the SMAWed sample of 14.5 %. When looking at the YS values, it can be observed that SMAWed sample obtain the highest value compared to the BM sample, which the YS value for SMAWed joint is 442 MPa, the YS value for BM is 302 MPa. A noticeable enhancement of approximately 59 % in the yield strength detected for the SMAWed joint over the Ys of the as received metal BM. The observed enhancement in yield stress may be attributed to the grain refinement in the WZ, [36].

Figure 9 shows SEM micrographs of the fracture area of the 2507 SDSS BM in the tensile test samples. The micrographs reveal elongated grains of both austenite (γ) and ferrite (α) phases aligned at a 45º degree angle, indicating the presence of ductile deformation in the BM sample as shown in figure 8 c. Ductile fractures are characterized by extensive plastic deformation and the presence of elongated dimples, deep dimples in various sizes and shapes (rounded and elongated) on the fracture surface. On the other hand, Figure 8b displays clear evidence of microstructural changes resulting from SMAWed. It is disclosed in the form of Shallow dimples and micro-cracks. Those features indicate ductile fracture mode. During the tensile test, the original microstructure experiences high stress, leading to significant plastic deformation. This induces distortions in the form of shallow dimples, as presents in figure 8d.

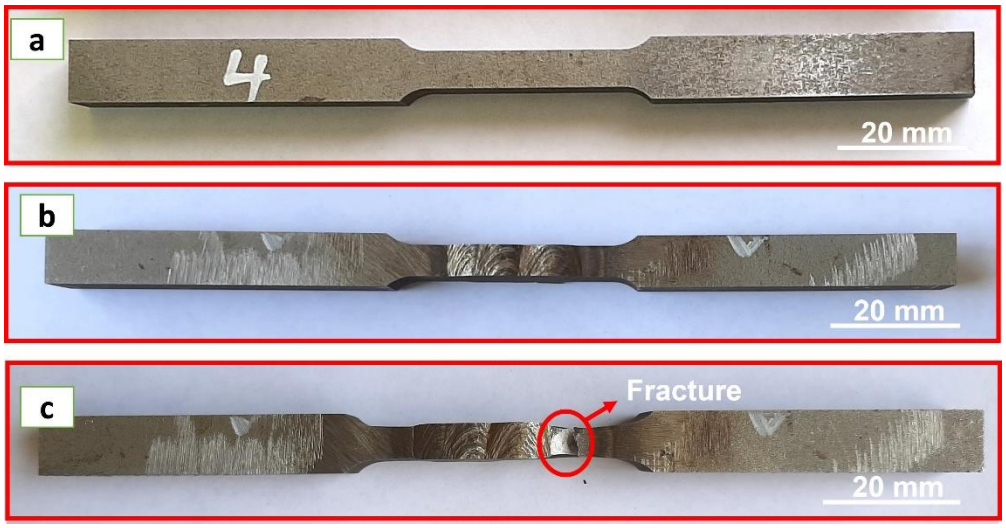

Fig. 7 (a) tensile test sample of the2507SDSS BM, (b) specimen of the SMAWed joint before tensile test (c) specimen of the welded joint after tensile test.

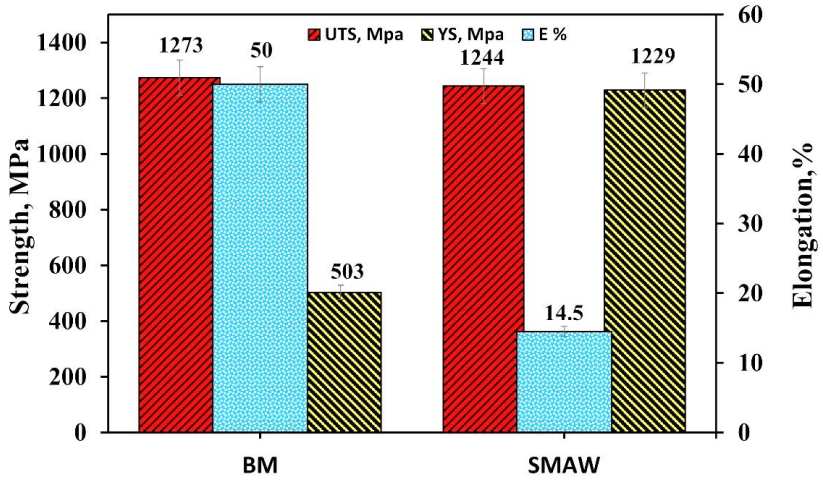

Fig. 8 Ultimate tensile stress, yield stress, and elongation properties of 2507 SDSS BM and SMAWed samples.

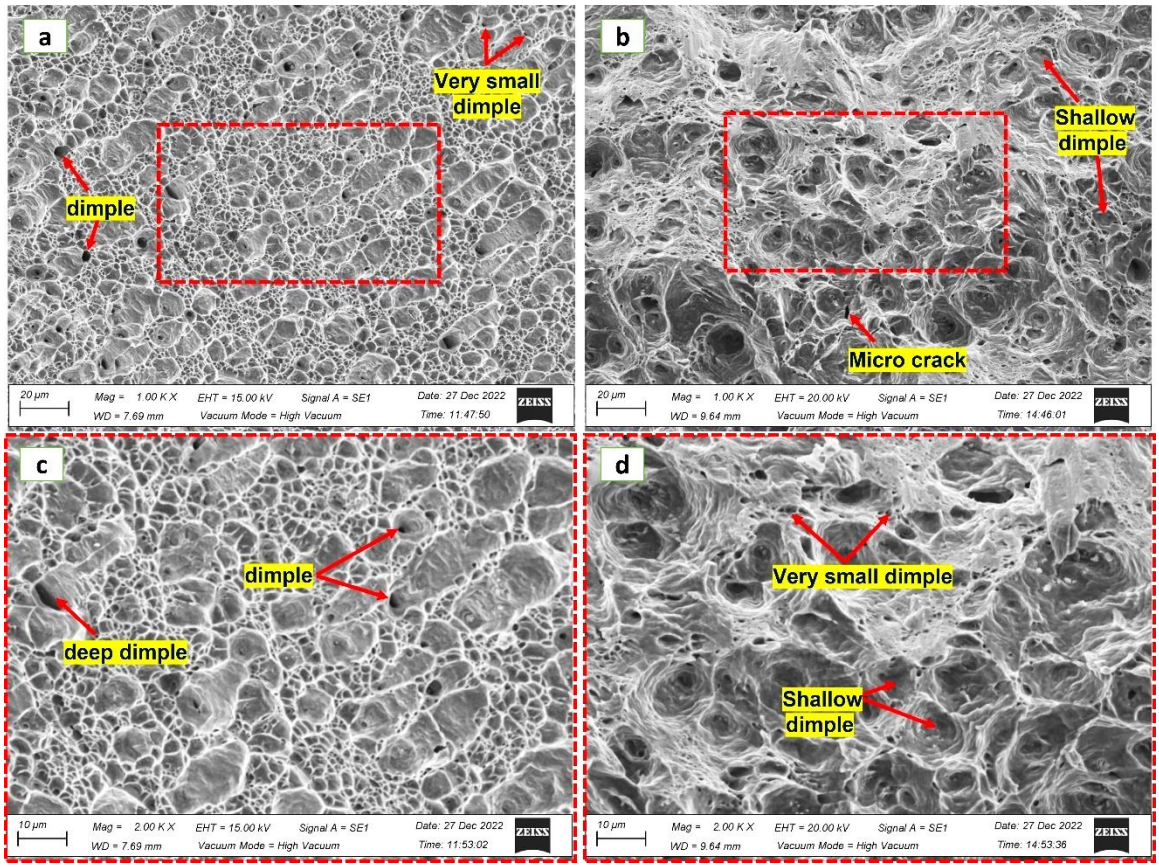

Fig. 9 SEM microphotographs of the fracture area of (a) BM, (b) the SMAWed sample, (c) a magnified image of the BM within the dashed rectangular area, and (d) a magnified image of the SMAWed sample within the dashed rectangular area.

CONCLUSIONS

The effect of different shieled metal arc welding parameters including filler electrode, heat inputs and interpass temperature on microstructure feature and mechanical properties of SMAWed 2507 SDSS were examined and evaluated. Based on the obtained results, the following conclusions can be stated:

1. Successful and defect-free joints of super-duplex stainless steels can be achieved by multi-pass shielded metal arc welding (SMAW) using ER2595 filler metal.

2. The weld zone microstructure exhibited four distinct morphologies of austenite including secondary austenite (SA), Widmanstatten austenite (WA), intra-granular austenite (IGA), and grain boundary austenite (GBA), in addition to the presence of ferrite.

3. Significant hardness enhancements have been observed in the weld zone for the SMAWed joint reached up to 369 HV compared to the BM of 319 HV.

4. The welded joint obtained ultimate tensile strength close to that of the BM, significant yield strength enhancements were observed compared to the BM. The yield strength of the welded joint is enhanced over the BM by 51%

5. The welding parameters affect the α and γ phase percentage within the weld zone. α and γ percentage phases for the SMAWed joint are 47% and 53 %, respectively. These phase ratios are relatively close to the equilibrium ratio of α and γ in the BM that achieves to 50.6% and 49.4%, respectively. These results endorse the use of multi pass SMAW for welding 2507 SDSS, specifically under the recommended welding parameters in the present study.

REFERENCES

1. Tiziani, R.C.P.F.A., "Annealing Temperature Effects on Super Duplex Stainless Steel UNS S32750 Welded Joints . I : Microstructure and Partitioning of Elements", 2010, pp. 4369 - 4377, doi:10.1007/s10853-010-4310-1.

2. Zhou, Y.; Zou, D.; Li, K.; Zhang, W.; Liu, R., "Effect of Cooling Time on Microstructure and Properties of 2507 Super Duplex Stainless Steel Welding Heat-Affect Zone. 2018, 940, pp. 53 - 58, doi:10.4028/www.scientific.net/MSF.940.53.

3. Sivagurumanikandan, N.; Saravanan, S.; Sivakumar, G.; Raghukandan, K. Process Window for Nd : YAG Laser Welding of Super Duplex Stainless Steel. 2018, 39, pp. 575 - 584, doi:10.1007/s10946-018-9754-9.

4. Beheshty, M.A.; Dehkordi, E.H.; Naghsh, K.Z.; Marnany, M.R.B. Effects of Welding Cycles on Microstructural Characteristics and Mechanical Properties of SAF 2507 Super Duplex Stainless Steel. 2018, 2, pp. 5 - 14.

5. Zhu, M.; He, F.; Yuan, Y.F.; Yin, S.M.; Guo, S.Y.; Pan, J. Effect of Aging Time on the Microstructure and Corrosion Behavior of 2507 Super Duplex Stainless Steel in Simulated Marine Environment. J. Mater. Eng. Perform. 2021, 30, pp. 5652 - 5666, doi:10.1007/s11665-021-05812-2.

6. Sun, Y.; Wu, X.; Wu, X.; Li, J.; Jiang, Y. Influence of Multi-Pass Welding on the Microstructure Evolution and Corrosion Resistance of a Super Duplex Stainless Steel. Int. J. Electrochem. Sci. 2016, 11, pp. 9666 - 9675, doi:10.20964/2016.11.28.

7. Kuroda, T.; Shimada, M. Micro Flash Butt Welding of Super Duplex Stainless Steel with Zr-Based Metallic Glass Insert. Vacuum 2008, 83, pp. 153 - 156, doi:10.1016/j.vacuum.2008.03.089.

8. Ahmed, M.M.Z.; Abdelazem, K.A.; El-Sayed Seleman, M.M.; Alzahrani, B.; Touileb, K.; Jouini, N.; El-Batanony, I.G.; Abd El-Aziz, H.M. Friction Stir Welding of 2205 Duplex Stainless Steel: Feasibility of Butt Joint Groove Filling in Comparison to Gas Tungsten Arc Welding. Materials (Basel). 2021, 14, pp. 1 - 21, doi:10.3390/ma14164597.

9. Taban, E. Toughness and Microstructural Analysis of Superduplex Stainless Steel Joined by Plasma Arc Welding. J. Mater. Sci. 2008, 43, pp. 4309 - 4315, doi:10.1007/s10853-008-2632-z.

10. Świerczyńska, A.; Łabanowski, J.; Fydrych, D. The Effect of Welding Conditions on Mechanical Properties of Superduplex Stainless Steel Welded Joints. Adv. Mater. Sci. 2014, 14, pp. 14 - 23, doi:10.2478/adms-2014-0002.

11. De Castro, J.A.; Oliveira, E.M.; Da Silva Almeida, D.S.; Da Fonseca, G.S.; Xavier, C.R. Effects of Local Heat Input Conditions on the Thermophysical Properties of Super Duplex Stainless Steels (SDSS). Mater. Res. 2017, 20, pp. 153–161, doi:10.1590/1980-5373-MR-2017-0384.

12. Datta, R.; Mukerjee, D.; Mishra, S. Weldability and Toughness Evaluation of

Pressure Vessel Quality Steel Using the Shielded Metal Arc Welding (SMAW) Process. J. Mater. Eng. Perform. 1998, 7, pp. 817 - 823, doi:10.1361 /105994998770347422.

13. Lippold, J.C. Characterization of Weld Solidification Cracking in a Duplex Stainless Steel Introduction Duplex Stainless Steels Have Become an Important Alternative to Con- Ventional Austenitic Stainless Steels in Marine , Petroleum , and Chemical Processing Applicatio. 1989, 19, pp. 1–19.

14. Frodigh, M.; Björnstedt, P.Å. Welding Guidelines for Duplex, Super Duplex and Hyper Duplex Stainless Steels. ESSC DUPLEX 2017 - 9th Eur. Stainl. Steel Conf. - Sci. Mark. 5th Eur. Duplex Stainl. Steel Conf. Exhib. 2017, 2017-May.

15. Valiente Bermejo, M.A.; Eyzop, D.; Hurtig, K.; Karlsson, L. Welding of Large Thickness Super Duplex Stainless Steel: Microstructure and Properties. Metals (Basel). 2021, 11, doi:10.3390/met11081184.

16. Westin, E.M.; Johansson, M.M.; Bylund, L.A.; Pettersson, R.F.A. Effect on Microstructure and Properties of Super Duplex Stainless Steel Welds When Using Backing Gas Containing Nitrogen and Hydrogen. Weld. World 2014, 58, pp. 347 - 354, doi:10.1007/s40194-014-0120-4.

17. Eghlimi, A.; Shamanian, M.; Raeissi, K. Effect of Current Type on Microstructure and Corrosion Resistance of Super Duplex Stainless Steel Claddings Produced by the Gas Tungsten Arc Welding Process. Surf. Coatings Technol. 2014, 244, pp. 45 - 51, doi:10.1016/j.surfcoat.2014.01.047.

18. Gupta, A.; Kumar, A.; Baskaran, T.; Arya, S.B.; Khatirkar, R.K. Effect of Heat Input on Microstructure and Corrosion Behavior of Duplex Stainless Steel Shielded Metal Arc Welds. Trans. Indian Inst. Met. 2018, 71, pp. 1595 - 1606, doi:10.1007/s12666-018-1294-z.

19. Abdelazem*, K.A.; El-Aziz, H.M.A.; Ahmed, M.M.Z.; El-Batanony, I.G. Characterization of Mechanical Properties and Corrosion Resistance of SAF 2205 Duplex Stainless Steel Groove Joints Welded Using Friction Stir Welding Process. Int. J. Recent Technol. Eng. 2020, 8, pp. 3428 - 3435, doi:10.35940/ijrte.f8502.038620.

20. Kumar, R.; Tewari, V.K.; Prakash, S. Oxidation Behavior of Base Metal, Weld Metal and HAZ Regions of SMAW Weldment in ASTM SA210 GrA1 Steel. J. Alloys Compd. 2009, 479, pp. 432 - 435, doi:10.1016/j.jallcom.2008.12.110.

21. Saxena, A.; Kumaraswamy, A.; Madhusudhan Reddy, G.; Madhu, V. Influence of Welding Consumables on Tensile and Impact Properties of Multi-Pass SMAW Armox 500T Steel Joints Vis-a-Vis Base Metal. Def. Technol. 2018, 14, pp. 188 - 195, doi:10.1016/j.dt.2018.01.005.

22. Balasubramanian, V.; Guha, B. Effect of L/T(p) Ratio on Fatigue Life Prediction of SMAW Cruciform Joints of ASTM 517 "F" Grade Steels. Int. J. Press. Vessel. Pip. 1998, 75, pp. 907 - 918, doi:10.1016/S0308-0161(98)00103-3.

23. Ahmed, S.R.; Agarwal, L.A.; Daniel, B.S.S. Correlation of Mechanical and Microstructural Properties in SMAW Welded Cr-Mo Boiler Steels Subjected to Different Post Weld Heat Treatment Soaking Times. Adv. Mater. Res. 2012, 585, pp. 425 - 429, doi:10.4028/www.scientific.net/AMR.585.425.

24. Aalami-Aleagha, M.E.; Rashidi, A.M. Correlated Macrostructural Parameters of Weld and Weld Current in the SMAW of Small Pipes. J. Mech. Sci. Technol. 2012, 26, pp. 181 - 185, doi:10.1007/s12206-011-0939-1.

25. Vimal, K.E.K.; Vinodh, S.; Raja, A. Optimization of Process Parameters of SMAW Process Using NN-FGRA from the Sustainability View Point. J. Intell. Manuf. 2017, 28, pp. 1459–1480, doi:10.1007/s10845-015-1061-5.
26. Khamari, B.K.; Dash, S.S.; Karak, S.K.; Biswal, B.B. Effect of Welding Parameters on Mechanical and Microstructural Properties of GMAW and SMAW Mild Steel Joints. Ironmak. Steelmak. 2020, 47, pp. 844–851, doi:10.1080/03019233.2019.1623592.
27. Kchaou, Y.; Haddar, N.; Hénaff, G.; Pelosin, V.; Elleuch, K. Microstructural, Compositional and Mechanical Investigation of Shielded Metal Arc Welding (SMAW) Welded Superaustenitic UNS N08028 (Alloy 28) Stainless Steel. Mater. Des. 2014, 63, pp. 278 - 285, doi:10.1016/j.matdes.2014.06.014.
28. Widodo, E.; Iswanto, I.; Nugraha, M.A.; Karyanik, K. Electric Current Effect on Mechanical Properties of SMAW-3G on the Stainless Steel AISI 304. MATEC Web Conf. 2018, 197, 1 - 4, doi:10.1051/matecconf/201819712003.
29. Mohandas, T.; Madhusudhan Reddy, G.; Naveed, M. Comparative Evaluation of Gas Tungsten and Shielded Metal Arc Welds of a `ferritic' Stainless Steel. J. Mater. Process. Technol. 1999, 94, pp. 133 - 140, doi:10.1016/S0924-0136(99)00092-8.
30. Migiakis, K.; Papadimitriou, G.D. Effect of Nitrogen and Nickel on the Microstructure and Mechanical Properties of Plasma Welded UNS S32760 Super-Duplex Stainless Steels. J. Mater. Sci. 2009, 44, pp. 6372–6383, doi:10.1007/s10853-009-3878-9.
31. ASTM E8 ASTM E8/E8M Standard Test Methods for Tension Testing of Metallic Materials 1. Annu. B. ASTM Stand. 4, 2010, pp. 1–27, doi:10.1520/E0008.
32. Arun, D.; Devendranath Ramkumar, K.; Vimala, R. Multi-Pass Arc Welding Techniques of 12 mm Thick Super-Duplex Stainless Steel. J. Mater. Process. Technol. 2019, 271, pp. 126–143, doi:10.1016/j.jmatprotec.2019.03.031.
33. Wang, L.; Zhao, P.; Pan, J.; Tan, L.; Zhu, K. Investigation on Microstructure and Mechanical Properties of Double-Sided Synchronous TIP TIG Arc Butt Welded Duplex Stainless Steel. Int. J. Adv. Manuf. Technol. 2021, 112, pp. 303–312, doi:10.1007/s00170-020-06375-7.
34. A Hosseini, V.; Hurtig, K.; Eyzop, D.; Östberg, A.; Janiak, P.; Karlsson, L. Ferrite Content Measurement in Super Duplex Stainless Steel Welds. Weld. World 2019, 63, pp. 551–563, doi:10.1007/s40194-018-00681-1.
35. Nowacki, J.; Łukojć, A. Structure and Properties of the Heat-Affected Zone of Duplex Steels Welded Joints. J. Mater. Process. Technol. 2005, 164–165, pp. 1074–1081, doi:10.1016/j.jmatprotec.2005.02.243.
36. Xie, X. fang; Li, J.; Jiang, W.; Dong, Z.; Tu, S.T.; Zhai, X.; Zhao, X. Nonhomogeneous Microstructure Formation and Its Role on Tensile and Fatigue Performance of Duplex Stainless Steel 2205 Multi-Pass Weld Joints. Mater. Sci. Eng. A 2020, 786, p. 139426, doi:10.1016/j.msea.2020.139426.